J. theor. Biol. (2001) **211,** 219–227
doi:10.1006/jtbi.2001.2340, available online at http://www.idealibrary.com on IDEAL®

Simulated Sinoatrial Exit Blocks Explained by Circle Map Analysis

PER ÖSTBORN*†, GUNNAR OHLÉN* AND BJÖRN WOHLFART‡

**Departments of Mathematical Physics, Lund University, S-221 00 Lund, Sweden and*
‡*Clinical Physiology, Lund University, S-221 00 Lund, Sweden*

(*Received on* 12 *June* 2000, *Accepted in revised form on* 24 *April* 2001)

In an accompanying study, it was seen that most cardiac arrhythmias that were simulated during poor intercellular coupling in the sinus node, were the same as those obtained in a two-element system in which one element suffered from a strong leakage current. This element corresponds to the sinus node periphery and is thus the one which feeds the atrium. In this paper, the interior element was replaced by a periodic stimulator. The dynamics of the peripheral element is then determined by its phase response curve. Phase response curves for sinus node elements subject to leakage were simulated for many different amplitudes of depolarizing stimuli. Simulations with circle maps based on these curves produced the same sequence of progressing levels of exit block as stimulus strength decreased, as did the two-element system when coupling strength was reduced. The bifurcations of the circle maps leading to the observed rhythms were identified. We found that the essential qualities of the phase response curves were determined by generally accepted properties of membrane currents. This suggests that the observed rhythms and bifurcations are generic.

Introduction

Circle maps give a new phase as a function of an old phase. They are thus one-dimensional maps. When these are used to model physical systems, they give the state of the system at discrete time t_{k+1} as a function of the state at time t_k, where the state is described by a single number (Kaplan & Glass, 1995). This is the simplest possible choice of a model. As such, it facilitates an understanding of the dynamics, provided that the essential qualities of the system can be carried into the map.

In an accompanying study, a two-element model of a weakly coupled sinus node (SN) was introduced. Element 1 corresponded to the SN interior, and element 2 to a slower peripheral SN domain. Element 2 was subjected to a strong leakage current, mimicking the influence from the atrium. In this study, element 1 is treated as a periodic stimulator, perturbing the slowly oscillating element 2.

Circle maps can be used to predict the response of an oscillator to periodic perturbation. The map then gives the phase in the cycle of the perturbed oscillator just before the $(n+1)$-th stimulus as a function of the phase just before the n-th. The experiments by Guevara *et al.* (1981) showed that the dynamics of periodically stimulated aggregates of automatic embryonic chick heart cells, was well mimicked by appropriate circle maps. This is due to the fact that oscillating cardiac cells return quickly to their limit cycles when perturbed. If the stimulation interval is not

†Author to whom correspondence should be addressed. E-mail: per.ostborn@matfys.lth.se

0022–5193/01/150219 + 09 $35.00/0

too short, they are therefore close to their limit cycle every time they are stimulated, and their state is well described by a single phase variable. In the language of dynamical system theory, they are strongly dissipative oscillators.

To construct appropriate circle maps, phase response curves (PRCs) are needed. These give the relative delay/advance of the subsequent upshot as a function of the phase of an injected stimulus. In the present study, the stimuli to the oscillator under consideration are intended to mimic those from central SN cells when they fire. The relevant PRCs are then those obtained when depolarizing pulses with a duration not far from that of an action potential are injected. Such PRCs have been experimentally measured by Sano *et al.* (1978) using aggregates of rabbit SN cells, and by Jalife *et al.* (1980) using aggregates of kitten SN cells. For a single rabbit SN cell, the PRC has been inferred from experiments in which the cell was periodically perturbed with different frequencies, and locked in different entrainment ratios (Anumonwo *et al.*, 1991). All these PRCs showed the same qualities (to be discussed below). These studies suggest that entrained cell aggregates respond to pulses in the same way as do single cells. This works in our favour, since the oscillator whose PRC we want to determine (element 2) is a peripheral SN frequency domain containing an unknown number of cells (see the accompanying paper). However, this domain differs from the cell aggregates in the studies mentioned above, in that it experiences a strong hyperpolarizing current. To our knowledge, no one has measured experimental PRCs under this condition. Therefore, we simulated them with the same version of the Irisawa & Noma (1982) SN element model as was used in the accompanying study.

Our intention was to investigate whether the PRC-based circle maps showed the same kind of rhythms when stimulus strength decreased as did the two-element- and network models of the SN when coupling conductance decreased. This was indeed the case, and since the dynamics of the circle maps is determined by the shape of the PRCs, this shape apparently determined the observed arrhythmias in the accompanying study. We analysed the origin of this shape, and the changes that occurred when stimulus strength was altered. The essential qualities could be traced back to generally accepted properties of membrane currents. This makes it plausible that the observed rhythms are generic during poor intercellular coupling in the SN. Because of their presumed generality, we also analysed the circle map bifurcations leading to these rhythms.

Methods

The peripheral SN element was simulated in the same way as element 2 in Fig. 5(a) of the accompanying paper. That is, the same simplified version of the SN element model of Irisawa & Noma (1982) was used. Q was set to 2, and a bias current of 1.4 A/F was added. The model was integrated with the forward Euler method with a time step of 1 ms. This led to a natural period $P_2 = 1952$ ms.

The symbols used in the definition of the PRC h are introduced in Fig. 1. h was defined as $h(\varphi) = T/P_2$, where $\varphi = t/P_2$, and $0 \leqslant t \leqslant P_2$. h is thus the ratio between the firing interval after perturbation (T) and the natural interval (P_2). The family of PRCs h for different pulse amplitudes A will be referred to as h_A. The value of h was simulated for pulses at 100 evenly spaced phases φ. The pulse width (70 ms) was chosen to approximately equal that of a perturbing action potential from the interior element 1.

The standard procedure to obtain the relevant circle map from the PRC is described below. Since it is assumed that element 2 is somewhere in its limit cycle every time it is perturbed, h can

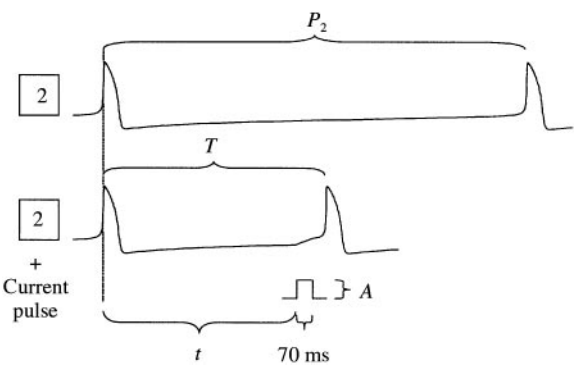

FIG. 1. Definition of the PRC $h(\varphi)$ for element 2. $\varphi = t/P_2$, where P_2 is the natural period of element 2. t is the time at which a square current pulse with duration 70 ms and amplitude A was delivered. $h(\varphi) = T/P_2$.

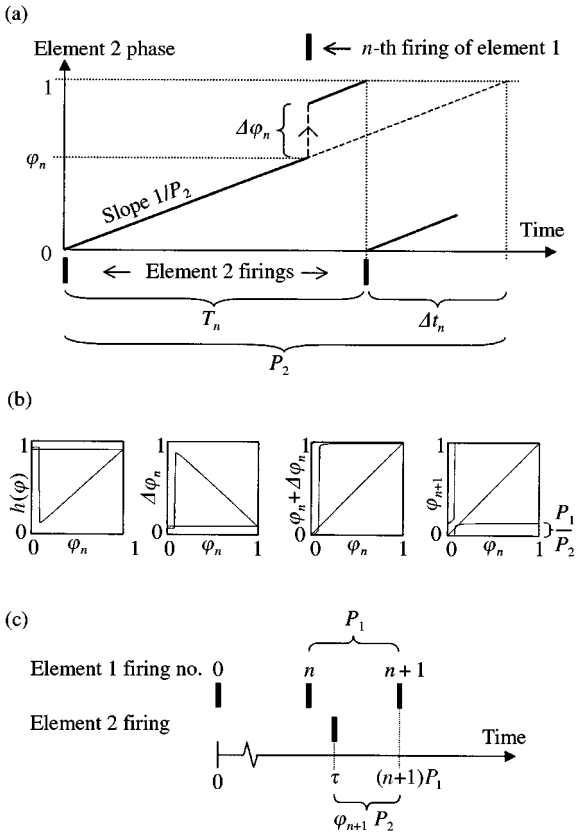

FIG. 2. How eqns (1) and (2) were obtained. (a) φ_n is the phase of element 2 just before element 1 fires for the n-th time. $\Delta\varphi_n$ is the immediate phase shift of element 2 when element 1 fires. T_n is the expected firing interval of element 2 (if element 1 does not fire again until element 2 fires the next time). Given the PRC $h(\varphi)$, $\Delta\varphi_n$ is obtained as $\Delta\varphi_n = (\mathrm{d}\varphi/\mathrm{d}t)\ \Delta t_n = (1/P_2)\ (P_2 - T_n) = 1 - h(\varphi_n)$. (b) Graphical illustration of the construction of the circle map M from h. (c) Determination of a firing instant τ of element 2 between the n-th and $(n+1)$-th firings of element 1, given φ_{n+1} [eqn (2)].

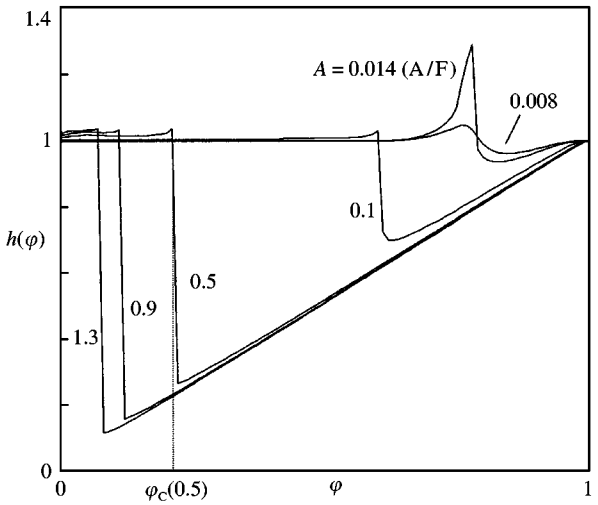

FIG. 3. The PRC h (Fig. 1) for different values of A. φ_c denotes the phase at which h crossed 1 from above. φ_c increased towards 1 as A decreased.

be interpreted as follows: when element 1 fires at phase φ in the cycle of element 2, the latter element stays in the cycle, but its phase immediately shifts to $\varphi + \Delta\varphi$, where $\Delta\varphi = 1 - h(\varphi)$ [Fig. 2(a)]. Otherwise, $\mathrm{d}\varphi/\mathrm{d}t = 1/P_2$. Then, if P_1 is the period of element 1, just before the next firing of this element, φ will have increased by the amount $P_1(\mathrm{d}\varphi/\mathrm{d}t) = P_1/P_2$. Thus,

$$\varphi_{n+1} = \left\{\varphi_n - \Delta\varphi_n + \frac{P_1}{P_2}\right\} \text{modulo } 1,$$

$$\Delta\varphi_n = 1 - h(\varphi_n), \qquad (1)$$

where φ_n is the phase in the cycle of element 2 just before the n-th firing of element 1. The modulo1 operation is performed since $0 \leqslant \varphi_n < 1$. Given h_A, eqn (1) defines a family of circle maps which will be referred to as M_A. Iterations of these maps were carried out using linear interpolation between the 100 measured points.

To construct a bifurcation diagram using eqn (1) corresponding to that in Fig. 5(a) in the accompanying paper, the sequence of firing intervals for element 2 is to be determined. This was done as follows: if $\varphi_n + \Delta\varphi_n + P_1/P_2 > 1$, then element 2 has fired between the n-th and $(n+1)$-th firing of element 1. The firing instant τ becomes [Fig. 2(c)]

$$\tau = (n+1)P_1 - \varphi_{n+1}P_2. \qquad (2)$$

The intervals I_k are then obtained as $I_k = \tau_{k+1} - \tau_k$.

Results

CIRCLE MAP DYNAMICS

A selection of PRCs for the peripheral element 2 from the family h_A is shown in Fig. 3.

The bifurcation diagram is shown in Fig. 4(a). Its structure was very similar to that of the original one [Fig. 5(a) in the accompanying paper], at least down to the 5:1 conduction zone. The

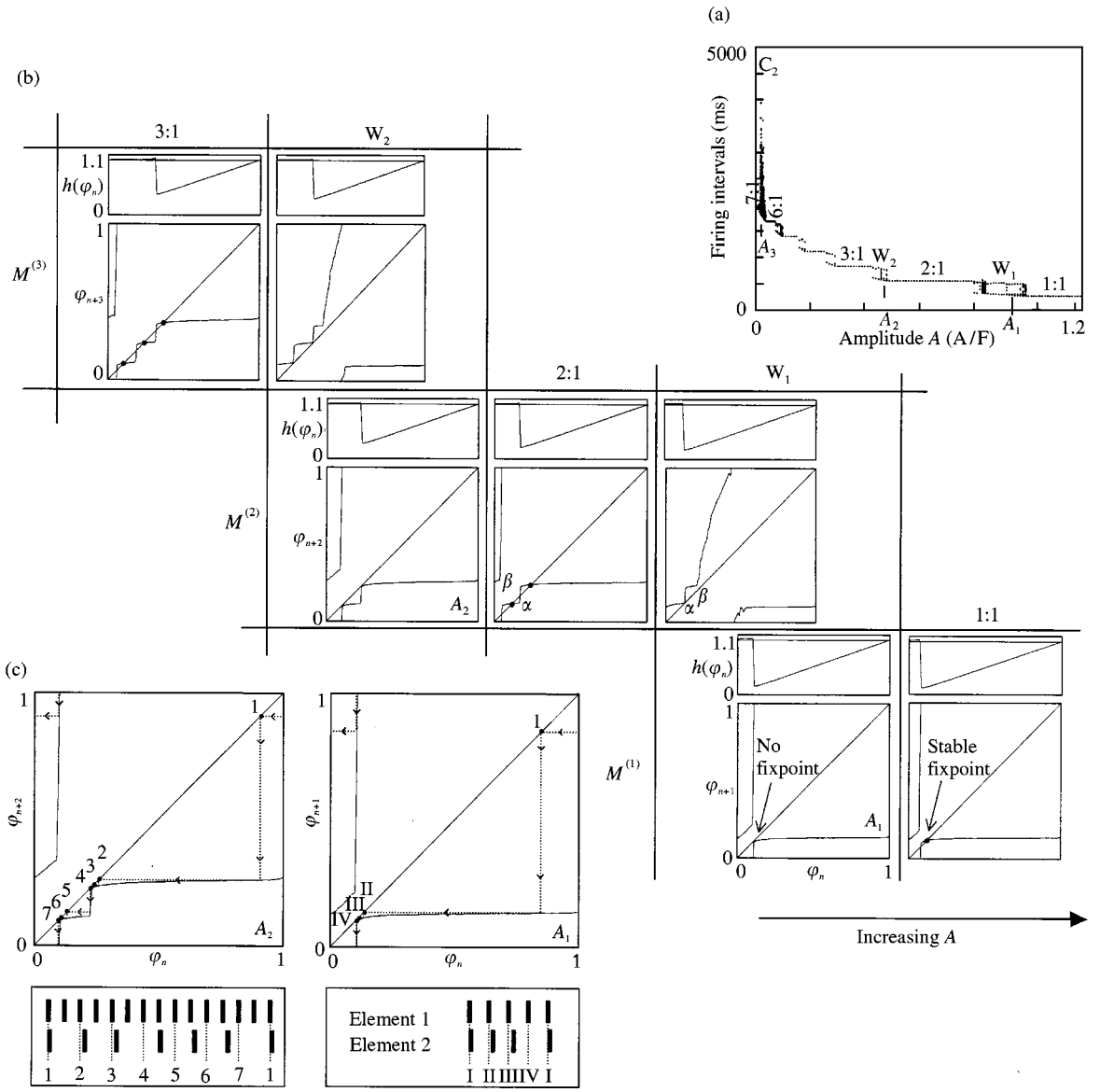

FIG. 4. (a) Bifurcation diagram corresponding to that in Fig. 5(a) in the accompanying paper, using eqns (1) and (2). The pulse amplitude A was bifurcation parameter instead of g. The dynamics at the marked amplitudes A_k was studied further (see also Fig. 5). (b) Circle maps $M^{(m)}$ in regions of the bifurcation diagram with different block patterns. Dots mark stable fixed points (see text). All bifurcations in these maps occurred since the vertical parts of $M^{(m)}$ moved to the right when φ_c grew as A decreased (compare the corresponding PRCs h on top). (c) M gave rise to a 4 : 3 Wenckebach rhythm at $A_1 = 0.94$ A/F (right panel), and $M^{(2)}$ produced a 7 : 3 W_2 rhythm at $A_2 = 0.46$ A/F (left panel). In the right panel the ever repeating phases I–IV are marked, and their relation to the 4 : 3 rhythm shown. In the left panel, the recurrent phases 1–7 are marked and their relation to the 7 : 3 rhythm shown.

W_1, W_2, W_3 and W_4 zones were successfully reproduced. The only difference was that for some parameter values in the circle map W_1 and W_2 zones, frequency locking was lost and we had quasi-periodic motion (Ott, 1993). The occurring intervals fill in vertical lines in Fig. 4(a). The prolonged irregular intervals in the C_2 zone were reproduced by M_A, while the C_1 zone was lacking. We note that frequency entrainment settled at 1 A/F. The amplitude of a model SN cell action potential is about 80 mV. If it had a square shape, it would give rise to a gap junction square current pulse with amplitude 1 A/F for $g = 12.5$ S/F. This is close to the true entrainment value

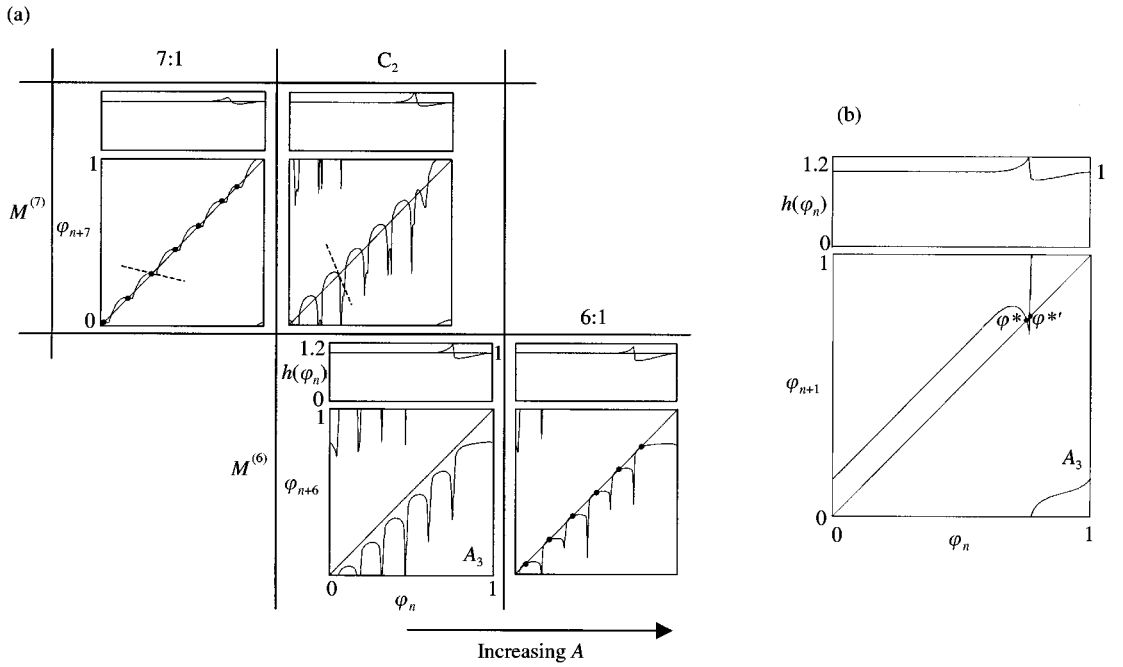

FIG. 5. The circle map C_2 region. (a) The region was entered when $M^{(6)}$ lost its six stable fixed points in a tangent bifurcation (bottom row). The 7 : 1 zone was entered when seven already existing fixed points in $M^{(7)}$ simultaneously became stable, that is, when the absolute value of the slope of $M^{(7)}$ at the fixed points became less than one (top row). (b) The map M at $A_3 = 0.026$ A/F, showing chaotic dynamics. The fixpoints φ^* and φ appeared because of the high peak in h (top). Periodic stimulation by element 1 starting *exactly* at one fixpoint makes element 2 quiescent. In practice, some very long firing intervals appeared (see text).

$g \approx 12$ S/F [Fig. 5(a) in the accompanying paper].

Figure 4(b) shows circle maps $M^{(m)}$ at different positions in the bifurcation diagram. These maps are defined according to the example $\varphi_{n+2} = M(\varphi_{n+1}) = M(M(\varphi_n)) = M^{(2)}(\varphi_n)$. Stable fixed points are marked with dots. That φ^* is a fixpoint of $M^{(m)}$ means that $\varphi^* = M^{(m)}(\varphi^*)$. φ^* is stable if and only if $|\mathrm{d}M^{(m)}/\mathrm{d}\varphi| < 1$ at φ^*. That is, points near φ^* will approach φ^* under iteration of $M^{(m)}$ if and only if this condition is fulfiled (Kaplan & Glass, 1995). If there is a periodic m: 1 block, then $M^{(m)}$ will have m stable fixed points, because then the system returns to its original state after m firings of element 1, so that we have $M^{(m)}(\varphi_n) = \varphi_{n+m} = \varphi_n$ for each of the m different phases occurring in this cycle.

Consider the maps M in Fig. 4(b) (bottom row). The vertical segment of M appears at the phase φ_c where h passes one from above. As A decreased, φ_c increased (compare the corresponding PRCs h on top). Thus, the vertical segment of M is shifted to the right. For the critical amplitude (coupling), this leads to loss of the stable fixpoint, and thus loss of 1 : 1 entrainment. An event of this kind is called a *tangent bifurcation*, since the graph is tangent to the diagonal at the critical amplitude. Looking at the maps $M^{(2)}$ in Fig. 4(b) (middle row), it is seen that the 2 : 1 block was created due to a tangent bifurcation in which two stable fixed points (and two unstable) appeared simultaneously†. This event took place because φ_c continued to grow as A decreased. The map moved to the right. At the critical amplitude, the two corners (α and β) of $M^{(2)}$ crossed the diagonal. In the 2 : 1 region, the second vertical segment of $M^{(2)}$ appeared at φ_c, and the first at its pre-image $M^{(-1)}(\varphi_c)$. As A decreased further—and φ_c increased—the drift to the right of $M^{(2)}$ continued. Finally the two stable fixed points were lost in a tangent bifurcation.

†The fixed points must appear simultaneously because $M^{(2)}$ cannot have a single fixpoint. If φ^* is a fixpoint of $M^{(2)}$, then $M(\varphi^*)$ must also be. Since M has no fixpoint for this A (there is no 1 : 1 entrainment), φ^* and $M(\varphi^*)$ must be distinct.

The same mechanism was responsible for the creation [Fig. 4(b), top row] and destruction of the 3:1 block region, and also for the 4:1, 5:1 and 6:1 regions. Four, five and six vertical segments of $M^{(4)}$, $M^{(5)}$ and $M^{(6)}$, respectively, drifted to the right because of their connection with φ_c. The reason why the width of the m:1 regions decreased with increasing m, is that φ_c increased with greater and greater speed when A decreased (Fig. 3), so that fixed points were created and destroyed more and more quickly.

Figure 4(c) shows how the W_1 and W_2 rhythms arose in M_A. At amplitude $A_1 = 0.94$ A/F, there was a 4:3 Wenckebach cycle (right panel). It is shown how the attractive set of ever repeating phases I–IV relates to the rhythm [compare with Fig. 5(b) in the accompanying paper]. The lost firing occurred when the orbit slipped through the narrow tunnel between the map graph and the diagonal. The closer A is to the bifurcation point, at which the fixpoint is lost, the narrower is the gap, and the more iterations are needed to pass it. More firings are transmitted before one is lost [Fig. 6 in the accompanying paper]. This mechanism behind Wenckebach rhythms has been described previously by Honerkamp (1983). The W_2 rhythms were Wenckebach-like since they were created in an analogous way. Considering $M^{(2)}$ instead of M, the map again had a near tangency with the diagonal and vertical segments. At $A_2 = 0.46$ A/F there was a 7:3 rhythm [Fig. 4(c), left panel]. The relation between the invariant phases 1–7 and the rhythm is shown [compare with Fig. 5(c) in the accompanying paper]. All the circle maps in the W_1 and W_2 regions were invertible, and thus the aperiodic behaviour seen for some A, as mentioned above, cannot be chaotic (Ott, 1993), but must be quasi-periodic. Considering the shape of $M^{(3)}$ [Fig. 4(b), top row], we see why the Wenckebach-like W_3 rhythms appeared after the loss of its three stable fixed points.

Figure 5(a) shows the appearance and disappearance of the region C_2 in M_A. As mentioned above, the 6:1 region was destroyed in a tangent bifurcation in which the six stable fixpoints of $M^{(6)}$ disappeared (bottom row). However, the 7:1 region was *not* created in a tangent bifurcation. Here, seven *already existing* fixed points of $M^{(7)}$ simultaneously became stable (top row).

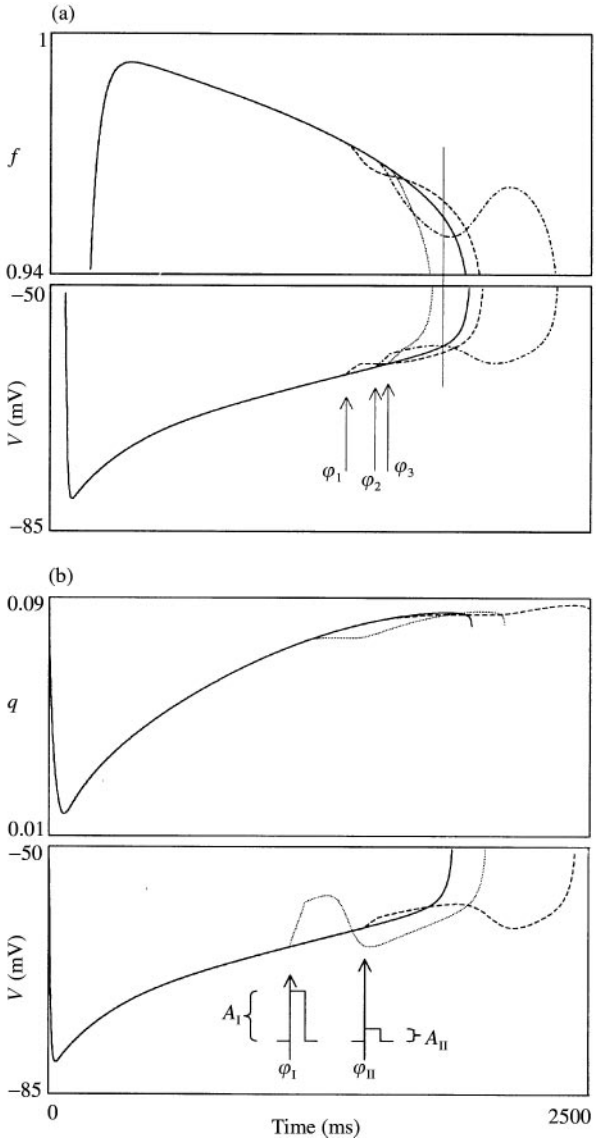

FIG. 6. (a) Qualitatively different responses to pulses with $A = 0.02$ A/F delivered to element 2 at $\varphi_1 = 0.7$, $\varphi_2 = 0.77$, and $\varphi_3 = 0.8$. At φ_1, a sub-threshold potential deflection and a small firing delay was produced. At φ_2, there was a super-threshold deflection, but no upshot, and a large delay. At φ_3, an upshot was triggered. Solid lines correspond to unperturbed activity. Top: Ca-inactivation f. Bottom: Membrane potential. The thin vertical line illustrates that after perturbation at φ_2 (dash–dotted lines), when potential has relaxed back to normal, f was still lower than normal (see text). (b) Effects of pulses delivered at phases $\varphi_I = 0.609$ and $\varphi_{II} = 0.780$ giving maximum firing delay for $A_I = 0.1$ and $A_{II} = 0.014$ A/F. Solid lines correspond to unperturbed activity. Top: i_h-activation variable q. Slow reactivation makes i_h stronger during the weaker pulse (see text). Bottom: Membrane potential.

These fixed points existed because of the seven dips in $M^{(7)}$, which were due to a dip in M. In Fig. 5(b), M is shown at $A_3 = 0.026$ A/F. The dip

in M is the high peak in h apparent for low amplitude pulses turned upside down (compare h on top). This peak thus made all maps $M^{(m)}$ non-invertible, thereby enabling chaotic dynamics (Ott, 1993). Iteration of M at A_3 from the initial condition $\varphi_0 = 0.2$ resulted in apparently chaotic motion with a positive Lyapunov exponent $\lambda = 0.24$. The Lyapunov exponent measures the exponential rate of divergence/convergence of the distance between two nearby iteration sequences. Since each iteration advances the system $P_1 = 280$ ms, the exponent for the flow would be $0.24/0.28 \approx 0.86\ \mathrm{s}^{-1}$.

Looking instead in the direction of increasing A, the 7 : 1 region was left after the seven fixpoints of $M^{(7)}$ became unstable as $\mathrm{d}M^{(m)}/\mathrm{d}\varphi$ dropped below -1. This is a *period-doubling bifurcation* (Ott, 1993), and is the beginning of a period-doubling cascade leading to chaos. The inset in Fig. 5(a) in the accompanying paper, shows that the C_2 region in the two-element system indeed was entered from the 7 : 1 region via an infinite sequence of period-doublings. This behaviour is thus explained by the appearance of the peak in h.

The peak in h was so high that it created two unstable fixed points φ^* and $\varphi^{*\prime}$ in M [Fig. 5(b)]. If element 2 is perturbed at, say, phase φ^* by element 1, its phase is shifted back ($\Delta\varphi < 0$) in such a way that when element 1 fires next time, it has just had time to regain phase φ^*. A paradoxical situation arises that repetitive stimulation may cause element 2 to never reach $\varphi = 1$, i.e. can make it quiescent. However, since φ^* is unstable, this situation will never occur in practice. Nevertheless, if we have chaotic dynamics, some phases in the iterations will come very close to φ^*. The following phases will then slowly slide away from φ^*, creating instead a very long firing interval. Qualitatively, this is probably the mechanism behind the long intervals appearing in the C_1 and C_2 regions in the original two-element system [Fig. 5(a) in the accompanying paper].

The C_1 region in the two-element system was also entered via a period doubling cascade [Fig. 5(a) in the accompanying paper]. Looking at $M^{(6)}$ in Fig. 5(a), we see that *if* its six dips had survived throughout the 6 : 1 region, then, as the map drifted to the left when A increased, the six fixed points would again have become unstable in a period doubling bifurcation. However, the dips happened to disappear before that, and therefore no C_1 region appeared in M_A.

RELATIONS BETWEEN PRC SHAPE AND MEMBRANE CURRENT DYNAMICS

We note first that PRCs obtained from normal model elements (without leakage) resemble those determined experimentally from rabbit SN by Sano *et al.* (1978) and from kitten SN by Jalife *et al.* (1980). Also, it was hard to distinguish the normal element PRCs resulting from our simplified Irisawa & Noma model from those obtained with the full model. These, and related quantities, are studied in detail by Guevara & Jongsma (1990).

Consider Fig. 3. All curves were bipolar, which means that $h > 1$ for $\varphi < \varphi_c$, and $h < 1$ for $\varphi > \varphi_c$. φ_c decreased with increasing A, but slower and slower, so that it reached an asymptotic value.

A study of the model variables revealed the following mechanism for the firing delay common for all A at very early phases. At the late stages of an upshot, the Ca-channel is inactivated to a large extent—that is, the variable f in the model is well below 1. Since the upshot is due to i_{Ca}, it is impossible to trigger the cell. Inactivation releases slowly when the potential drops. If a depolarizing pulse arrives, release is delayed. For some time, i_{Ca} will be weaker than normal. Since this current is important for the slow diastolic depolarization, the firing threshold will be reached later.

On the other hand, if the pulse comes late enough (after φ_c), the only effect is that of triggering. We get $h < 1$.

Now consider a pulse injected at a phase just before φ_c, which does not bring the potential to firing threshold, but just below. The potential increase accelerates the slow Ca-channel inactivation. Due to the slow release of this inactivation when potential relaxes back, and the potential becomes identical with the one obtained if no pulse was applied, f will have a lower value than in the unperturbed case. The action potential will again be delayed. This situation is illustrated in Fig. 6(a). After perturbation at phase φ_2 (dash–dotted lines), the potential became identical with the unperturbed one (solid

line) at the thin vertical line. However, the perturbed value of f was considerably lower at this moment.

The qualitatively different responses to perturbations just before and just after φ_c produced an almost vertical segment of h (for appreciable A). This segment was essential for the creation of the Wenckebach rhythms shown in Fig. 4(c).

Clearly, since the potential gap to firing threshold increases from zero when φ decreases from 1, φ_c continuously decreases from 1 with increasing pulse amplitude A. The reason why the rate of decrease dropped, is that the temporal increase in i_{Ca} during the pulse was lower if initial potential was lower, since then we fell more below the Ca-channel activation threshold. Therefore a pulse of given strength received less and less help from i_{Ca} in order to raise potential to firing threshold when φ decreased. That φ_c decreased more slowly with A for higher A was the reason why the $m:1$ conduction plateaux in Fig. 4(a) were wider for higher A (lower m).

The most remarkable thing about the PRCs is the high peak appearing before φ_c for *weak* pulses (Fig. 3). Consider again Fig. 6(a). A pulse applied at φ_1 produced a sub-threshold potential deflection, in the sense that it relaxed back immediately after the pulse ended. f was only moderately reduced, and the subsequent upshot only slightly delayed. A pulse at φ_3 triggered an action potential. The pulse at φ_2 produced a super-threshold response, but *the leakage was so strong* that it competed with the activated Ca-current, preventing the formation of an upshot. The only effect was the long-lasting Ca-current inactivation, leading to a long firing delay.

We think the reason why this effect was much more pronounced for weak pulses is to be found in the dynamics of the hyperpolarization-activated current i_h. This current was essential for the slow diastolic depolarization in the drained model element, being about twice as strong as i_{Ca} at this stage. It activated with a very long time constant (2–3 s) after a firing (Irisawa & Noma, 1982), so that its activation variable q increased throughout the slow depolarization [Fig. 6(b)]. For weaker pulses, φ_c and the peak in the PRC appeared for later phases. Therefore, after the pulse, q was higher and i_h stronger. It therefore helped to keep up the potential in the super-threshold deflection for a longer time, leading to a later renormalization of membrane activity and a longer firing delay. In Fig. 6(b) are shown the potentials when pulses were applied at the phases producing maximum firing delay for $A = 0.1$ A/F (dotted lines) and $A = 0.014$ A/F (dashed line). In the top panel, it is seen that q stayed at a higher value for the weaker pulse.

For stronger pulses, the curves h_A did not exceed 1 much. They were almost horizontal for $\varphi < \varphi_c$. This leads to invertible maps M, which exclude chaotic dynamics. The reason for this flatness of h is simply that the moderate firing delays are divided with a very long natural period P_2. The lack of chaos in the two-element system for higher conductances g is therefore probably a model-independent property.

Discussion

The validity of the two-element model of the SN was discussed in the accompanying paper. Here we discuss the simplifying assumptions needed to transform this system into circle maps. We also identify which PRC qualities were vital for the appearance of the bifurcation diagram [Fig. 5(a) in the accompanying paper, and Fig. 4(a) in this paper].

The reason why element 1 could be approximated by a periodic simulator is that for a leakage current so large that it almost prevents a cell from firing spontaneously, such as the one flowing out of element 2, the firing interval of this cell increases rapidly with the leakage (Watanabe *et al.*, 1995). In other words, small currents have large effect on the intervals. Thus a pulse delivered by element 1 has much larger effect on the firing intervals of element 2 than vice versa. Element 2 tends to fire soon after a firing of element 1. Either element 2 is triggered, or the leakage prevents it from reaching threshold before the next perturbation from element 1. This element will therefore be perturbed only at small phases in its cycle. Such perturbations only produce small changes in the firing interval (see Fig. 3 or the experimental PRCs in Sano *et al.*, 1978 or Jalife *et al.*, 1980).

As mentioned before, the circle map approach can only be successful if the perturbed oscillator is close to its limit cycle every time it is

stimulated. The similarity between the bifurcation diagram in this study [Fig. 4(a)], and the two-element diagram in the accompanying paper, in itself confirms this assumption. However, for the weaker pulse in Fig. 6(b) it is seen that element 2 certainly did not return close to the limit cycle within the period 280 ms of element 1. The potential trace seemed to regain normal shape after ~ 600 ms, and q stayed higher than normal in the whole time range. Therefore, in the very weak amplitude region, the map does not apply for phases φ_n at which we are close to the top of the high peak in h. This is probably the reason why M_A does not reproduce the chaotic region C_2 with quantitative accuracy, and C_1 not at all.

The PRC qualities (Fig. 3) essential for the appearance of the bifurcation diagrams (Fig. 4 in this paper, and Fig. 5 in the accompanying one) were identified to be: (1) that $h > 1$ for small phases and $h < 1$ for larger phases, (2) that h was vertical at this polarity shift, (3) that the vertical segment moved to the right when pulse amplitude decreased, (4) that it moved with greater and greater speed, (5) that h had a high peak for very weak pulses, and (6) that it did not exceed 1 significantly for greater amplitudes. The causes of these qualities are analysed above, and we argue that they are quite model independent. Qualities (1)–(3) were seen in all experimental PRC measurements mentioned in the introduction.

Due to the possible relevance to SA exit block rhythms, we think that experiments measuring PRCs of SN cells subject to a strong hyperpolarizing current are called for. In particular, it would be interesting to see whether the curious high peak in the weak pulse PRCs arises in experiment also. This peak was responsible for the chaotic rhythms in the bifurcation diagram.

This study was supported by the Swedish Medical Research Council (Grant No 14X-08664).

REFERENCES

ANUMONWO, J. M. B., DELMAR, M., VINET, A., MICHAELS, D. C. & JALIFE, J. (1991). Phase resetting and entrainment of pacemaker activity in single sinus node cells. *Circ. Res.* **68,** 1138–1153.

GUEVARA, M., GLASS, L. & SHRIER, A. (1981). Phase locking, period-doubling bifurcations, and irregular dynamics in periodically stimulated cardiac cells. *Science* **214,** 1350–1352.

GUEVARA, M. R. & JONGSMA, H. J. (1990). Phase resetting in a model of sinoatrial nodal membrane: ionic and topological aspects. *Am. J. Physiol.* **258,** H734–H747.

HONERKAMP, J. (1983). The heart as a system of coupled nonlinear oscillators. *J. Math. Biol.* **18,** 69–88.

IRISAWA, H. & NOMA, A. (1982). Pacemaker mechanisms of rabbit sinoatrial node cells. In: *Cardiac Rate and Rhythm*, (Bouman, L. N. & Jongsma, H. J., eds). The Hague: Nijhoff, p. 35–51.

JALIFE, J., HAMILTON, A. J., LAMANNA, V. R. & MOE, G. K. (1980). Effects of current flow on pacemaker activity of the isolated kitten sinoatrial node. *Am. J. Physiol.* **238,** H307–H316.

KAPLAN, D. & GLASS, L. (1995). *Understanding nonlinear dynamics.* New York: Springer-Verlag.

MICHAELS, D. C., MATYAS, E. P. & JALIFE, J. (1986). Dynamic interactions and mutual synchronization of sinoatrial node pacemaker cells. A mathematical model. *Circ. Res.* **58,** 706–720.

OTT, E. (1993). *Chaos in Dynamical Systems.* Cambridge: Cambridge University Press.

SANO, T., SAWANOBORI, T. & ADANIYA, H. (1978). Mechanisms of rhythm determination among pacemaker cells of the mammalian sinus node. *Am. J. Physiol.* **235,** H379–H384.

SOEN, Y., COHEN, N., LIPSON, D. & BRAUN, E. (1999). Emergence of spontaneous rhythm disorders in self-assembled networks of heart cells. *Phys. Rev. Lett.* **82,** 3556–3559.

TAKAHASHI, N., HANYU, Y., MUSHA, T., KUBO, R. & MATSUMOTO, G. (1990). Global bifurcation structure in periodically stimulated giant axons of squid. *Physica D* **43,** 318–334.

WATANABE, E. I., HONJO, H., ANNO, T., BOYETT, M. R., KODAMA, I. & TOYAMA, J. (1995). Modulation of pacemaker activity of sinoatrial node cells by electrical load imposed by an atrial cell model. *Am. J. Physiol.* **269,** H1735–H1742.